Mon. Not. R. Astron. Soc. **398,** 2152–2165 (2009) doi:10.1111/j.1365-2966.2009.15265.x

The structure of blue supergiant winds and the accretion in supergiant high-mass X-ray binaries

L. Ducci,[1,2]★ L. Sidoli,[2] S. Mereghetti,[2] A. Paizis[2] and P. Romano[3]

[1]*Dipartimento di Fisica e Matematica, Università degli Studi dell'Insubria, Via Valleggio 11, I-22100 Como, Italy*
[2]*INAF, Istituto di Astrofisica Spaziale e Fisica Cosmica, Via E. Bassini 15, I-20133 Milano, Italy*
[3]*INAF, Istituto di Astrofisica Spaziale e Fisica Cosmica, Via U. La Malfa 153, I-90146 Palermo, Italy*

Accepted 2009 June 17. Received 2009 June 16; in original form 2009 May 5

ABSTRACT

We have developed a stellar wind model for OB supergiants to investigate the effects of accretion from a clumpy wind on the luminosity and variability properties of high-mass X-ray binaries. Assuming that the clumps are confined by ram pressure of the ambient gas and exploring different distributions for their mass and radii, we computed the expected X-ray light curves in the framework of the Bondi–Hoyle accretion theory, modified to take into account the presence of clumps. The resulting variability properties are found to depend not only on the assumed orbital parameters but also on the wind characteristics. We have then applied this model to reproduce the X-ray light curves of three representative high-mass X-ray binaries: two persistent supergiant systems (Vela X−1 and 4U 1700−377) and the supergiant fast X-ray transient IGR J11215−5952. The model can reproduce the observed light curves well, but requiring in all cases an overall mass loss from the supergiant about a factor of 3–10 smaller than the values inferred from ultraviolet lines studies that assume a homogeneous wind.

Key words: supergiants – X-rays: individual: Vela X−1/4U 1900−40, 4U 1700−377, IGR J11215−5952.

1 INTRODUCTION

A new class of massive X-ray binaries has been recognized in the last few years, mainly thanks to observations carried out with the *INTEGRAL* satellite. They are transient X-ray sources associated with O or B supergiant stars and characterized by short outbursts. These *supergiant fast X-ray transients* (SFXTs) (Sguera et al. 2005; Negueruela et al. 2006) are remarkably different from the classical high-mass X-ray binaries (HMXBs) with supergiant companions, that are bright persistent sources, and also differ from the Be transients for their optical companions and shorter outbursts.

The outbursts of SFXTs involve a high dynamic range, spanning three to five orders of magnitudes, from a quiescent luminosity of $\sim 10^{32}$ erg s^{-1} up to the peak luminosity of 10^{36}–10^{37} erg s^{-1}. The outbursts typically last a few days and are composed of many short flares with duration of a few hours. Besides these bright outbursts, the SFXTs can display a fainter flaring activity with luminosity $L_{\rm X} = 10^{33}$–10^{34} erg s^{-1} (Sidoli et al. 2008). Different mechanisms have been proposed to explain the SFXT properties (see Sidoli 2009 and references therein for a recent review).

Sidoli et al. (2007) proposed that SFXT outbursts are due to the presence of an equatorial wind component, denser and slower than the spherically symmetric wind from the supergiant, and possibly inclined with respect to the orbital plane of the system. The enhanced accretion rate occurring when the neutron star crosses this wind component can explain SFXTs showing periodic outbursts, such as IGR J11215−5952 and also other SFXTs, assuming different geometries for the outflowing equatorial wind.

Another possibility involves the gated mechanisms due to transitions across the centrifugal barrier (Grebenev & Sunyaev 2007). Bozzo, Falanga & Stella (2008) showed that a centrifugal or a magnetic barrier can explain the SFXT properties only if the supergiant wind is inhomogeneous, and the accreting neutron star has a strong magnetic field ($\gtrsim 10^{14}$ G) and a long spin period ($P_{\rm spin} \geq 10^3$ s).

in't Zand (2005) proposed that the SFXT flares are produced by accretion of clumps of matter from the companion wind. In the framework of the clumpy wind model proposed by Oskinova, Hamann & Feldmeier (2007), Walter & Zurita Heras (2007) and Negueruela et al. (2008) proposed that what distinguishes the SFXTs from the persistent HMXBs with supergiant companions is their different orbital separation: in persistently bright sources, the compact object orbits the companion at a small distance (<2 stellar radii) where there is a high number density of clumps, while the transient emission in SFXTs is produced by accretion of much rarer clumps present at larger distances. On the other hand, the monitoring with *Swift* of a sample of four SFXTs (Sidoli et al. 2008) has demonstrated that these sources also accrete matter outside the bright outbursts, so any model should also account for this important observational property.

★E-mail: lorenzo@iasf-milano.inaf.it

The winds of O- and B-type stars are driven by the momentum transfer of the radiation field, and Lucy & Solomon (1970) showed that the dominant mechanism is the line scattering. The analytical formulation for line-driven winds has been developed by Castor, Abbott & Klein (1975, hereafter CAK). In the CAK theory, the mass lost by the star is smoothly accelerated by the momentum transferred from the stellar continuum radiation, and forms a stationary and homogeneous wind. However, both observational evidence and theoretical considerations indicate that the stellar winds are variable and non-homogeneous. Changes in the ultraviolet (UV) line profiles, revealing wind variability, have been observed on time-scales shorter than a day (Kudritzki & Puls 2000). The X-ray variability observed in 4U 1700−377, Vela X−1 and other HMXBs can be explained in terms of wind inhomogeneity (White, Kallman & Swank 1983; Kreykenbohm et al. 2008), and further indications for the presence of clumps come from X-ray spectroscopy. For example, the X-ray spectrum of Vela X−1 during the eclipse phase shows recombination lines produced by a hot ionized gas and fluorescent K-shell lines produced by cool and dense gas of near-neutral ions (Sako et al. 1999). These authors proposed that the coexistence of highly ionized and near-neutral ions can be explained with an inhomogeneous wind, where cool, dense clumps are embedded in a lower density, highly ionized medium.

Lucy & White (1980) suggested that the wind acceleration is subject to a strong instability, since small perturbations in the velocity or density distribution grow with time producing a variable and strongly structured wind. The first time-dependent hydrodynamical simulations of unstable line-driven winds were performed by Owocki, Castor & Rybicki (1988) and, more recently, by Runacres & Owocki (2002) and Runacres & Owocki (2005). All these simulations show that the line-driven instability produces a highly structured wind, with reverse and forward shocks that compress the gas into clumps. Moreover, the shock heating can generate a hot interclump medium into which the colder clumps are immersed (Carlberg 1980).

Based on these considerations, we study in this work the expected variability and X-ray luminosity properties of neutron stars accreting from a clumpy wind. In the next two sections, we describe our clumpy wind model and the assumptions for the mass accretion. In Section 4, we study the dependence of the parameters introduced in the previous sections. In Sections 5–7, we compare the X-ray light curves predicted with our model to the observations of three HMXBs, showing that it is possible to reproduce the observed flaring behaviours well.

2 CLUMPY STELLAR WIND PROPERTIES

In our model, where the dynamical problem has not been treated, we assume that a fraction of the stellar wind is in the form of clumps with a power-law mass distribution

$$p(M_{\rm cl}) = k \left(\frac{M_{\rm cl}}{M_{\rm a}}\right)^{-\zeta} \tag{1}$$

in the mass range $M_{\rm a}$–$M_{\rm b}$. The rate of clumps produced by the supergiant is related to the total mass-loss rate $\dot{M}_{\rm tot}$ by

$$\dot{N}_{\rm cl} = \frac{f\dot{M}_{\rm tot}}{\langle M\rangle} \text{ clumps s}^{-1}, \tag{2}$$

where $f = \dot{M}_{\rm cl}/\dot{M}_{\rm tot}$ is the fraction of mass lost in clumps and $\langle M\rangle$ is the average clump mass, which can be computed from equation (1).

Clumps are driven radially outwards by absorption of UV spectral lines (CAK). From spectroscopic observations of O stars, Lépine & Moffat (2008) suggest that clumps follow on average the same velocity law of a smooth stellar wind. We can then assume the following clump velocity profile without solving the dynamical problem:

$$v_{\rm cl}(r) = v_\infty \left(1 - 0.9983\frac{R_{\rm OB}}{r}\right)^{\beta}, \tag{3}$$

where v_∞ is the terminal wind velocity, $R_{\rm OB}$ is the radius of the supergiant, 0.9983 is a parameter which ensures that $v(R_{\rm OB}) \approx 10$ km s^{-1} and β is a constant in the range $\sim$ 0.5–1.5 (Kudritzki et al. 1989; Lamers & Cassinelli 1999).

Assuming that the clumps are confined by the ram pressure of the ambient gas, their size can be derived by the balance pressure equation. Following Lucy & White (1980) and Howk et al. (2000), the average density of a clump is

$$\bar{\rho}_{\rm cl} = \rho_{\rm w}(r)\left(\frac{a_{\rm w}^2 + C_\rho\omega^2}{a_{\rm c}^2}\right), \tag{4}$$

where $\rho_{\rm w}(r)$ is the density profile of the homogeneous (interclump) wind, $a_{\rm w}$ and $a_{\rm c}$ are the interclump wind and the clump thermal velocity, respectively: $a_{\rm w}^2 = \frac{kT_{\rm w}}{\mu m_{\rm H}}$ and $a_{\rm c}^2 = \frac{kT_{\rm c}}{\mu m_{\rm H}}$. k is the Boltzmann constant, $T_{\rm w}$ and $T_{\rm c}$ are the temperatures of the interclump wind and of the clumps, respectively, and μ is the mean atomic weight. The constant $C_\rho = 0.29$ accounts for the confining effect of the bow shock produced by the ram pressure around the clump (Lucy & White 1980). ω is the relative velocity between the wind and the clump ($\omega = v_{\rm w} - v_{\rm cl}$). Adopting $\bar{\omega} \sim 5 \times 10^7$ cm s^{-1}, $\bar{T}_{\rm c} \sim 10^5$ K, $\bar{T}_{\rm w} \sim 10^7$ K and $\mu = 1.3$, we obtain[1]

$$\left(\frac{a_{\rm w}^2 + C_\rho\omega^2}{a_{\rm c}^2}\right) \approx 200. \tag{5}$$

Since the density radial profile $\rho_{\rm w}(r)$ of the homogeneous interclump wind (obtained from the continuity equation $\dot{M} = 4\pi r^2\rho_{\rm w}(r)v(r) =$ constant) is

$$\rho_{\rm w}(r) = \rho_{\rm w}(r_0)\frac{r_0^2 v(r_0)}{r^2 v(r)}, \tag{6}$$

where r_0 is a generic distance from the supergiant, from equations (4)–(6), we obtain

$$\bar{\rho}_{\rm cl}(r) = \bar{\rho}_{\rm cl}(r_0)\frac{r_0^2 v(r_0)}{r^2 v(r)}, \tag{7}$$

where $\bar{\rho}_{\rm cl}(r_0) = \rho_{\rm w}(r_0) \times (a_{\rm w}^2 + C_\rho\omega^2)/a_{\rm c}^2$. Bouret, Lanz & Hillier (2005) analysed the far-UV spectrum of O-type supergiants and found that clumping starts deep in the wind, just above the sonic point $R_{\rm s}$, at velocity $v(R_{\rm s}) \approx 30$ km s^{-1}. In the CAK model, the sonic point is defined as the point where the wind velocity is equal to the sound speed [$v(R_{\rm s}) = c_{\rm s}$]:

$$R_{\rm s} = \frac{0.9983R_{\rm OB}}{1 - (c_{\rm s}/v_\infty)^{1/\beta}}. \tag{8}$$

Adopting typical parameters for O supergiants, from equation (8) we obtain that the clumping phenomenon starts close to the photosphere ($R_{\rm s} \approx R_{\rm OB}$).

Assuming spherical geometry for the clumps and that the mass of each clump is conserved, it is possible to obtain the expansion law of the clumps from equation (7), with $r_0 = R_{\rm s}$:

$$R_{\rm cl}(r) = R_{\rm cl}(R_{\rm s})\left[\frac{r^2 v_{\rm cl}(r)}{R_{\rm s}^2 v(R_{\rm s})}\right]^{1/3}. \tag{9}$$

[1] This value is just an estimate of a typical value of ratio of clump to ambient density, and will not be adopted throughout.

From equation (9), we find that the clump size increases with the distance from the supergiant star.

For the initial clump dimensions, we tried two different distributions, a power law

$$\dot{N}_{M_{\rm cl}} \propto R_{\rm cl}^{\gamma} \text{ clumps s}^{-1} \tag{10}$$

and a truncated Gaussian function

$$\dot{N}_{M_{\rm cl}} \propto \frac{1}{\sigma\sqrt{2\pi}} \mathrm{e}^{-\frac{1}{2}\left(\frac{R_{\rm cl}-\bar{R}_{\rm cl}}{\sigma}\right)^2} \text{ clumps s}^{-1}, \tag{11}$$

where $\sigma = (R_{\rm cl,max} - R_{\rm cl,min})/(2N_\sigma)$ and N_σ is a free parameter.

For any given mass clump, we derived the minimum and maximum values for the initial radii as follows. The minimum radius is that below which the clump is optically thick for the UV resonance lines. In this case, gravity dominates over the radiative force causing the clump to fall back on to the supergiant. The momentum equation of a radiatively driven clump is

$$v_{\rm cl}\frac{{\rm d}v_{\rm cl}}{{\rm d}r} = -\frac{GM_{\rm OB}}{r^2} + g_{\rm e} + g_{\rm L}, \tag{12}$$

where $M_{\rm OB}$ is the mass of the supergiant, $g_{\rm e}$ is the radiative acceleration due to the continuum opacity by electron scattering, $g_{\rm L}$ is the radiative acceleration due to line scattering. While equation (12) is an approximation that ignores the pressure gradient, the solution of the momentum equation differs only slightly from the accurate solution derived by Kudritzki et al. (1989); another assumption is that the photosphere has been treated as a point source (Lamers & Cassinelli 1999).

The radiative acceleration due to electron scattering is

$$g_{\rm e}(r) = \frac{\sigma_{\rm e}(r)L_{\rm OB}}{4\pi r^2 c}, \tag{13}$$

where $\sigma_{\rm e}$ is the opacity for electron scattering, and is given by $\sigma_{\rm e} = \sigma_{\rm T}\frac{n_{\rm e}}{\rho_{\rm cl}}$, where $\sigma_{\rm T}$ is the Thomson cross-section, $n_{\rm e}$ is the number density of electrons, $\rho_{\rm cl}$ is the density of the clump and $L_{\rm OB}$ is the luminosity of the OB supergiant. Lamers & Cassinelli (1999) found $0.28 < \sigma_{\rm e} < 0.35$ cm^2 g^{-1}. Assuming a constant degree of ionization in the wind, both $\sigma_{\rm e}$ and $g_{\rm e}$ are constant.

The radiative acceleration due to the line scattering is

$$g_{\rm L} = \frac{\sigma_{\rm e}^{\rm ref}L_{\rm OB}}{4\pi c r^2} k t^{-\alpha}\left(10^{-11}\frac{n_{\rm e}}{W}\right)^{\delta}, \tag{14}$$

where $\sigma_{\rm e}^{\rm ref} = 0.325$ cm^2 g^{-1}, k, α, δ are the force multiplier parameters, which are obtained with the calculation of the line radiative force (Abbott 1982). t is the dimensionless optical depth parameter (CAK). According to the model of Howk et al. (2000), we assume no velocity gradient inside the clump (of size $l \approx 2R_{\rm cl}$), then we utilize the dimensionless optical depth parameter for a static atmosphere $t = \sigma_{\rm e}\int_l \rho\,{\rm d}r.W(r)$ is the geometrical dilution factor (Lamers & Cassinelli 1999), given by

$$W(r) = \frac{1}{2}\left[1 - \sqrt{1 - \left(\frac{R_{\rm OB}}{r}\right)^2}\right]. \tag{15}$$

According to equation (7), we find that the number density of electrons in each clump is given by

$$n_{\rm e}(r) = n_0\frac{R_{\rm s}^2 v(R_{\rm s})}{r^2 v(r)}, \tag{16}$$

where $n_0 = n_{\rm e}(R_{\rm s})$, such that

$$n_0 = \frac{\rho_{\rm cl}(R_{\rm s})}{\mu_{\rm e} m_{\rm H}}. \tag{17}$$

From equation (12), we obtain that the minimum radius of the clump is given by

$$g_{\rm L} + g_{\rm e} - g_{\rm g} = 0, \tag{18}$$

where $g_{\rm g}$ is the acceleration due to gravity. Approximating t as

$$t \approx \sigma_{\rm e}\frac{M_{\rm cl}}{V_{\rm cl}}2R_{\rm cl} = \frac{3}{2}\sigma_{\rm e}\frac{M_{\rm cl}}{\pi R_{\rm cl}^2} \tag{19}$$

and assuming the force multiplier parameters calculated by Shimada et al. (1994), with $v(R_{\rm s}) = 30$ km s^{-1} and $r_0 = R_{\rm s}$, we finally obtain the lower limit for the clump radius:

$$R_{\rm cl,min}(M_{\rm cl}) = \left(\frac{AB}{C}\right)^{1/(3\delta-2\alpha)}, \tag{20}$$

where

$$A = \left(\frac{3\sigma_{\rm e}M_{\rm cl}}{2\pi}\right)^{-\alpha}, \tag{21}$$

$$B = \left[\frac{3M_{\rm cl}10^{-11}}{4\pi\mu_{\rm e}m_{\rm H}W(R_{\rm s})}\right]^{\delta}, \tag{22}$$

$$C = (g_{\rm g} - g_{\rm e})\frac{4\pi c R_{\rm S}^2}{\sigma_{\rm e}^{\rm ref}L_{\rm OB}\dot{k}} \tag{23}$$

We found that for the interesting range of the clump masses, the drag force (Lucy & White 1980) values are less than 3 per cent of the forces resulting from equations (13) and (14). Thus, in the determination of the minimum clump radius, we can neglect this contribution.

The upper limit to the clump radius is obtained from the definition of a clump as an overdensity with respect to the interclump smooth wind:

$$\rho_{\rm cl} \geq \frac{\dot{M}_{\rm w}}{4\pi R_{\rm s}^2 v_{\rm w}(R_{\rm s})}, \tag{24}$$

where $\dot{M}_{\rm w}$ is the mass-loss rate of the homogeneous wind component (interclump). From equation (24), we obtain the upper limit for the clump radius

$$R_{\rm cl,max}(M_{\rm cl}) = \left[\frac{3M_{\rm cl}R_{\rm S}^2 v_{\rm w}(R_{\rm s})}{\dot{M}_{\rm w}}\right]^{1/3}. \tag{25}$$

The lower and the upper limits for the clump radius (equations 20 and 24) depend on the supergiant parameter $T_{\rm eff}$, $L_{\rm OB}$, $R_{\rm OB}$, v_∞, β and $\dot{M}_{\rm w}$. Thus, supergiants of different spectral types have, for any given mass of the clump, different minimum and maximum values for the initial radius distribution. However, these differences are smaller than a factor of 10 for OB supergiants, and the intersection of the upper- and lower-limit functions ranges from $M_{\rm cl} \approx 10^{20}$ to 10^{23} g.

3 LUMINOSITY COMPUTATION

The Bondi–Hoyle–Lyttleton accretion theory (Hoyle & Lyttleton 1939; Bondi & Hoyle 1944) is usually applied to the HMXBs where an OB supergiant loses mass in the form of a fast stellar wind (terminal velocity, $v_\infty \approx$ 1000–2000 km s^{-1}) that is assumed to be homogeneous and spherically symmetric. Only matter within a distance smaller than the *accretion radius* ($R_{\rm a}$) is accreted:

$$R_{\rm a}(r) = \frac{2GM_{\rm NS}}{v_{\rm rel}^2(r) + c_{\rm s}^2}, \tag{26}$$

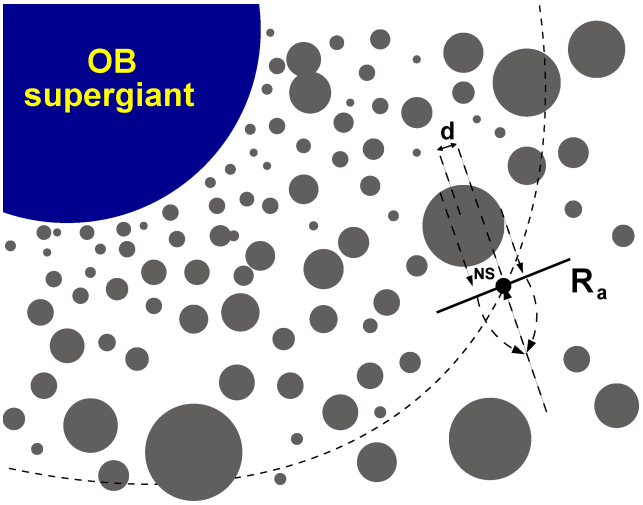

Figure 1. Schematic representation of our clumpy wind model. d is the distance between the centre of the clump and the centre of accreting compact object. R_a is the accretion radius.

where M_{NS} is the neutron star mass and $v_{rel}(r)$ is the relative velocity between the neutron star and the wind. The fraction of stellar wind gravitationally captured by the neutron star is given by

$$\dot{M}_{accr} = \rho_{wind}(r) v_{rel}(r) \pi R_a^2, \tag{27}$$

where $\rho_{wind}(r)$ is the density of the wind (Davidson & Ostriker 1973).

The Bondi–Hoyle–Lyttleton accretion theory, that is based on a homogeneous wind, requires an important modification to properly take into account the presence of inhomogeneity in a clumpy wind. In the homogeneous case, the wind particles are deflected by the gravitational field of the neutron star, and collide with the particles having the symmetric trajectory in a cylindrical region with axis along the relative wind direction. The collisions dissipate the kinetic energy perpendicular to this axis, and only the particles with a parallel kinetic energy component lower than the gravitational potential energy are accreted. The application of this accretion mechanism to an inhomogeneous wind can lead to a partial accretion of the clump: when the distance d between the neutron star and the projection of the centre of the clump on the accretion cross-section is smaller than the clump radius and $d \neq 0$, only a fraction of the mass of the clump will be accreted (see Fig. 1). In particular, if an incoming clump that crosses the accretion cross-section πR_a^2 is smaller than the accretion radius ($R_{cl} < R_a$) and $d < R_{cl}$, the accretion cross-section in equation (27) must be replaced by

$$\Sigma = 4 \int_d^{R_{cl}} \sqrt{R_{cl}^2 - x^2}\,dx \tag{28}$$

and the mass accretion rate is $\dot{M}_{accr} = \rho_{cl}(r) v_{rel}(r) \times \Sigma$ (see Fig. 2A). If $R_{cl} \geq R_a$, we have three cases:

(i) when $R_{cl} - d \geq R_a$ (Fig. 2B), the accretion cross-section is given by

$$\Sigma = \pi R_a^2; \tag{29}$$

(ii) when $R_{cl} - d < R_a$ and $\sqrt{R_{cl}^2 - d^2} < R_a$ (Fig. 2C), the accretion cross-section is given by equation (28);

(iii) when $R_{cl} - d < R_a$ and $\sqrt{R_{cl}^2 - d^2} > R_a$ (Fig. 2D), the accretion cross-section is given by

$$\Sigma = 4 \left[\int_{x_{int}}^{R_{cl}} \sqrt{R_{cl}^2 - x^2}\,dx - (x_{int} - d) y_{int} + \int_{y_{int}}^{R_a} \sqrt{R_a^2 - y^2}\,dy \right]. \tag{30}$$

The number density of clumps n_{cl} obeys the equation of continuity $\dot{N}_{cl} = 4\pi r^2 n_{cl}(r) v_{cl}(r)$, where $\dot{N}_{cl}$ is the rate of clumps emitted by the OB supergiant (see equation 1). Thus,

$$n_{cl}(r) = \frac{\dot{N}_{cl}}{4\pi r^2 v_{cl}(r)} \text{ clumps cm}^{-3}. \tag{31}$$

The rate of clumps accreted by the neutron star is given by

$$\dot{N}_{accr} = n_{cl}(r) v_{rel}(r) \times \left(\pi R_a^2\right) \text{ clumps s}^{-1}. \tag{32}$$

When the neutron star accretes only the interclump wind, the X-ray luminosity variations are due to changes in its distance from the OB companion due to orbital eccentricity. The corresponding luminosity (see equations 26 and 27) is

$$L_{X,wind}(\phi) = \frac{G M_{NS}}{R_{NS}} \dot{M}_{accr} = \frac{(G M_{NS})^3}{R_{NS}} \frac{4\pi \rho_w(r)}{\left[(v_{rel}^2(r) + c_s^2\right]^{3/2}}, \tag{33}$$

where ϕ is the orbital phase and $\rho_w(r)$ is given by equation (6).

When the neutron star accretes a clump, its X-ray luminosity is given by

$$L_{X,cl}(\phi) = \frac{G M_{NS}}{R_{NS}} \frac{M_{cl}}{\frac{4}{3}\pi R_{cl}^3} v_{rel} \times \Sigma, \tag{34}$$

where $R_{cl}(r)$ is given by equation (9), and Σ by equations (28)–(30). If two or more clumps are accreted at the same time, the X-ray luminosity at the peak of the flare produced by the accretion is

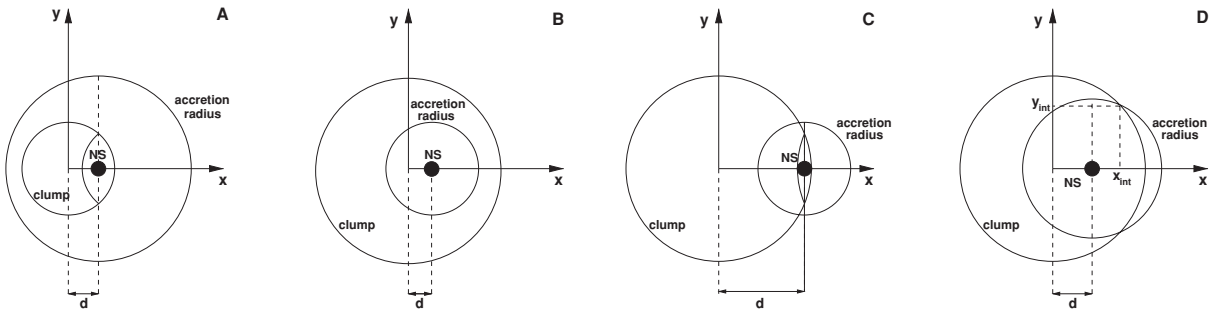

Figure 2. Schematic view of different possibilities for the accretion of clumps of radius R_{cl}. (A): $R_{cl} \leq R_a$ and $d \neq 0$ (equation 28); (B): $R_{cl} > R_a$ and $R_{cl} - d \geq R_a$ (equation 29); (C): $R_{cl} - d < R_a$ and $\sqrt{R_{cl}^2 - d^2} < R_a$ (equation 28); (D): $R_{cl} - d < R_a$ and $\sqrt{R_{cl}^2 - d^2} > R_a$ (equation 30).

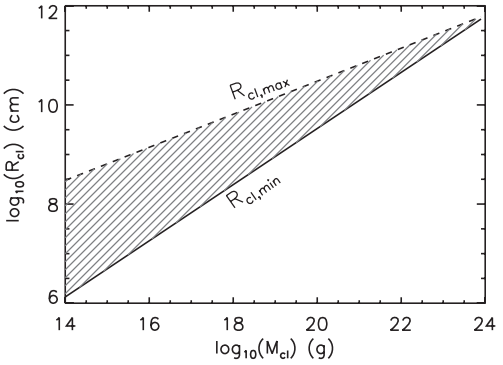

Figure 3. Upper limit (dashed line) and lower limit (solid line) for the clump radius at $r = R_s$. They have been obtained from equations (20) and (25) assuming the following parameters for the supergiant: $M_{OB} = 30\,M_\odot$, $R_{OB} = 23.8\,R_\odot$, $\dot{M}_{tot} = 10^{-6}\,M_\odot\,yr^{-1}$, $v_\infty = 1700\,km\,s^{-1}$, $\beta = 1$, $v_0 = 10\,km\,s^{-1}$ and $\dot{M}_{cl}/\dot{M}_{wind} = 0.7$.

given by the sum of the luminosities (equation 34) produced by the accretion of each clump.

4 APPLICATION OF THE CLUMPY WIND MODEL

In this section, we investigate how the X-ray luminosity and variability properties depend on the different clumpy wind parameters and orbital configurations.

As an example, we consider a binary consisting of an O8.5I star with $M_{OB} = 30\,M_\odot$, $R_{OB} = 23.8\,R_\odot$ (Vacca, Garmany & Shull 1996) and a neutron star with $M_{NS} = 1.4\,M_\odot$, $R_{NS} = 10$ km. The parameters for the supergiant wind are as follows: $\dot{M}_{tot} = 10^{-6}\,M_\odot\,yr^{-1}$ (Puls et al. 1996), $v_\infty = 1700\,km\,s^{-1}$, $\beta = 1$, $v_0 = 10\,km\,s^{-1}$, and the force multiplier parameters are $k = 0.375$, $\alpha = 0.522$ and $\delta = 0.099$ (Shimada et al. 1994). The corresponding upper and lower limits to the clump radius, derived from equations (20) and (25), are shown in Fig. 3.

4.1 The effect of the mass distribution

To study the effects of the clump masses, we computed the distributions of the flare luminosity and durations for different values of ζ, f, M_a and M_b considering for simplicity a circular orbit with $P_{orb} = 10$ d. We first neglected the clump radius distribution assuming that clumps which start from the sonic radius have radii given by equation (20), and follow the expansion law (equation 9). We found that when M_a and/or M_b increase, the number of clumps produced by the supergiant decreases (see equation 2), resulting in a smaller number of X-ray flares. The average flare luminosity, the average flare duration, the number of flares and the shapes of the luminosity and flare duration distributions do not change much for different values of M_a and M_b. In Fig. 4, we show the dependence of the distributions of flare luminosities and durations on ζ and f (for $M_a = 10^{19}$ g, $M_b = 10^{22}$ g). If ζ increases, the number of clumps and their density increase (see equations 2 and 20), implying a higher number of flares, a shift to higher luminosities and to shorter flare durations.

Fig. 5 shows the effect of changing the fraction of wind mass in the form of clumps f for different values of ζ. When f increases, the supergiant produces more clumps (see equation 2), thus the number of flares and their average luminosity increase, while their average duration remains unchanged.

4.2 The effect of the radius distribution

In Section 2, we showed that, for any given mass, the clump dimensions are constrained within the limits given by equations (20) and (25). Here, we show the effect of different assumptions on the radius distribution laws. We considered both a power law (equation 10) and a truncated normal distribution (equation 11), described by the parameters γ (or N_σ). When γ increases, the number of clumps with larger density decreases, thus the average luminosity of the flares decreases and their average duration increases (see Fig. 6). We also found that when ζ increases, the flare distributions with a positive γ follow a different behaviour than those with a negative value: for $\gamma < 0$, the flare distributions behave as described above (i.e. the number of flares increases with ζ), while this does not happen for $\gamma > 0$. This is due to the fact that in this case the clumps are larger, thus there is a high probability that two or more clumps overlap thus reducing the number of flares.

For the case of a normal distribution of clump radii, we calculated the distributions of flare luminosities and durations for different values of N_σ (see Fig. 7). When N_σ increases, the number of clumps with larger and smaller radii is reduced, resulting in a narrower flare luminosity distribution. When ζ increases, the flare distributions have the same behaviour described above for the case $\gamma > 0$.

We then tried another test, increasing the orbital period (e.g. from 10 to 100 days), finding that the shape of the integral distributions in Fig. 6 remains similar, except for the number of X-ray flares which decreases.

4.3 The effect of the mass-loss rate

The effects of different wind mass-loss rates $\dot{M}_{tot}$ are shown in Fig. 8. The mass-loss rate is usually derived observationally from the strength of the Hα emission line, since this gives smaller uncertainties than the method based on UV P-Cygni lines (Kudritzki & Puls 2000). Since the Hα line opacity depends on ρ^2, the presence of wind inhomogeneities leads to an overestimate of the mass-loss rate. In particular, the mass-loss rates from O stars derived from smooth-wind models measurements with the Hα method need to be reduced by a factor of 3–10 if the wind is clumpy (see Lépine & Moffat 2008 and Hamann, Feldmeier & Oskinova 2008). In Fig. 8, we show that if $\dot{M}_{tot}$ decreases, also the number of flares decreases due to the reduced number of clumps. Also, the average luminosity of the flares is reduced because the number density of clumps decreases resulting in a smaller probability that two or more clumps overlap.

4.4 The effect of the orbital parameters

In Fig. 9, we show the effect of changing the orbital period P_{orb} and the eccentricity e. We assumed $\zeta = 1.1$, $\gamma = -1.5$, $f = 0.7$. When the orbital period increases, the number of flares emitted by the neutron star decreases (see equation 31) and the neutron star accretes clumps with a smaller density (see equation 9), implying a shift to lower luminosities and higher flare durations (see Fig. 9). When the eccentricity increases, the neutron star accretes clumps with a higher density range (in general, clumps are denser when they are closer to the supergiant), thus the luminosity range of the flares increases, as shown in Fig. 9.

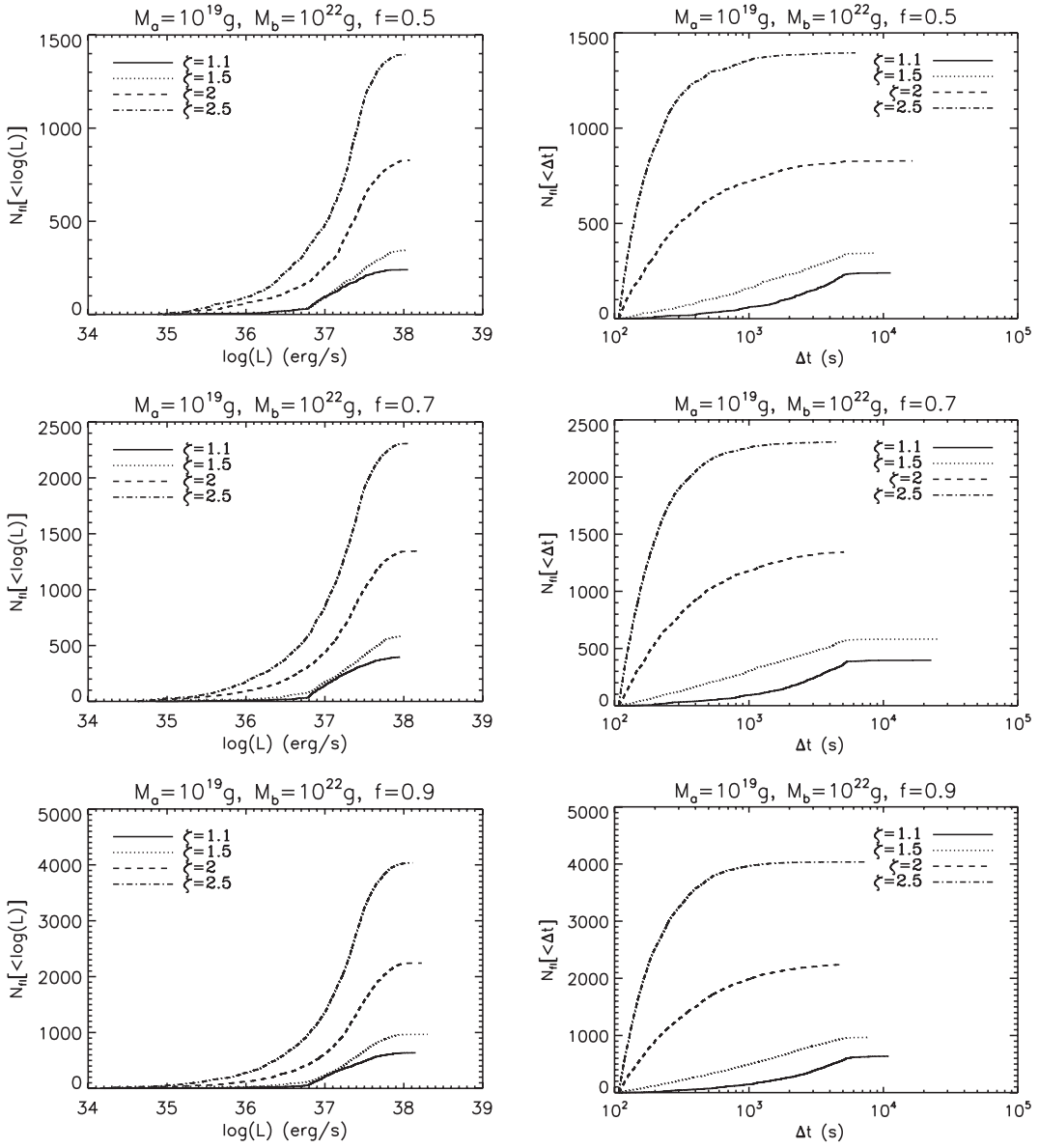

Figure 4. Expected integral distributions of the flare luminosities (left-hand panels) and durations (right-hand panels) for different values of ζ and $f = \dot{M}_{\rm cl}/\dot{M}_{\rm tot}$. The binary system parameters are as follows: $M_{\rm OB} = 30\,{\rm M}_\odot$, $R_{\rm OB} = 23.8\,{\rm R}_\odot$, $M_{\rm NS} = 1.4\,{\rm M}_\odot$, $R_{\rm NS} = 10$ km, $P_{\rm orb} = 10$ d and $e = 0$. The parameters for the supergiant wind are as follows: $\dot{M}_{\rm tot} = 10^{-6}\,{\rm M}_\odot\,{\rm yr}^{-1}$, $v_\infty = 1700\,{\rm km\,s}^{-1}$, $\beta = 1$, $v_0 = 10\,{\rm km\,s}^{-1}$, $M_{\rm a} = 10^{19}$ g and $M_{\rm b} = 10^{22}$ g and $f = 0.5, 0.7, 0.9$. The time interval for each histogram corresponds to 100 days.

5 COMPARISON WITH THE HMXB VELA X−1

Vela X−1 (4U 1900−40) is a bright eclipsing X-ray binary ($P_{\rm orb} = 8.964$ d, $e \sim 0.09$) formed by the B0.5 Ib supergiant HD 77581 (Brucato & Kristian 1972) ($M = 23\,{\rm M}_\odot$, $R = 30\,{\rm R}_\odot$; van Kerkwijk et al. 1995) and a pulsar with spin period ∼283 s and mass $1.9\,{\rm M}_\odot$. This source shows significant X-ray variability on short time-scales, with flares lasting from ∼500 to 40 000 s (Haberl 1994; Kreykenbohm et al. 2008).

Recently, Kreykenbohm et al. (2008) analysed *INTEGRAL* observations of Vela X−1 obtained during a phase of high flaring activity, finding two kinds of flares: brief and bright flares softer than longer flares. They also found several off-states, during which the source is not detected (at least by *INTEGRAL*). Kreykenbohm et al. (2008) proposed that the short flares are caused by the flip–flop instability, while the long ones are due to the accretion of clumps ejected by the supergiant. The off-states are explained as due to the onset of the propeller effect when the neutron star crosses the lower density interclump medium.

In this section, we apply our wind model to Vela X−1, assuming the wind parameters derived by Searle et al. (2008) and reported in Table 1.

In Fig. 10, we compare the light curve measured with the All Sky Monitor (ASM)/*RXTE* instrument with that calculated with our clumpy wind model assuming a spherical symmetry for the outflowing wind. The ASM/*RXTE* count rate, measured in the 2–10 keV range, has been converted to the 1–100 keV luminosity using the average spectral parameters obtained by Orlandini et al. (1998) and the distance of 2 kpc (Sadakane et al. 1985). The observed light curve of Vela X−1 is well reproduced by our clumpy wind model for $\dot{M}_{\rm tot} = 2.1 \times 10^{-7}\,{\rm M}_\odot\,{\rm yr}^{-1}$, $M_{\rm a} = 5 \times 10^{18}$ g and $M_{\rm b} = 5 \times 10^{21}$ g, $\zeta = 1.1$, $f = 0.75$ and $\gamma = -1$. Acceptable light curves

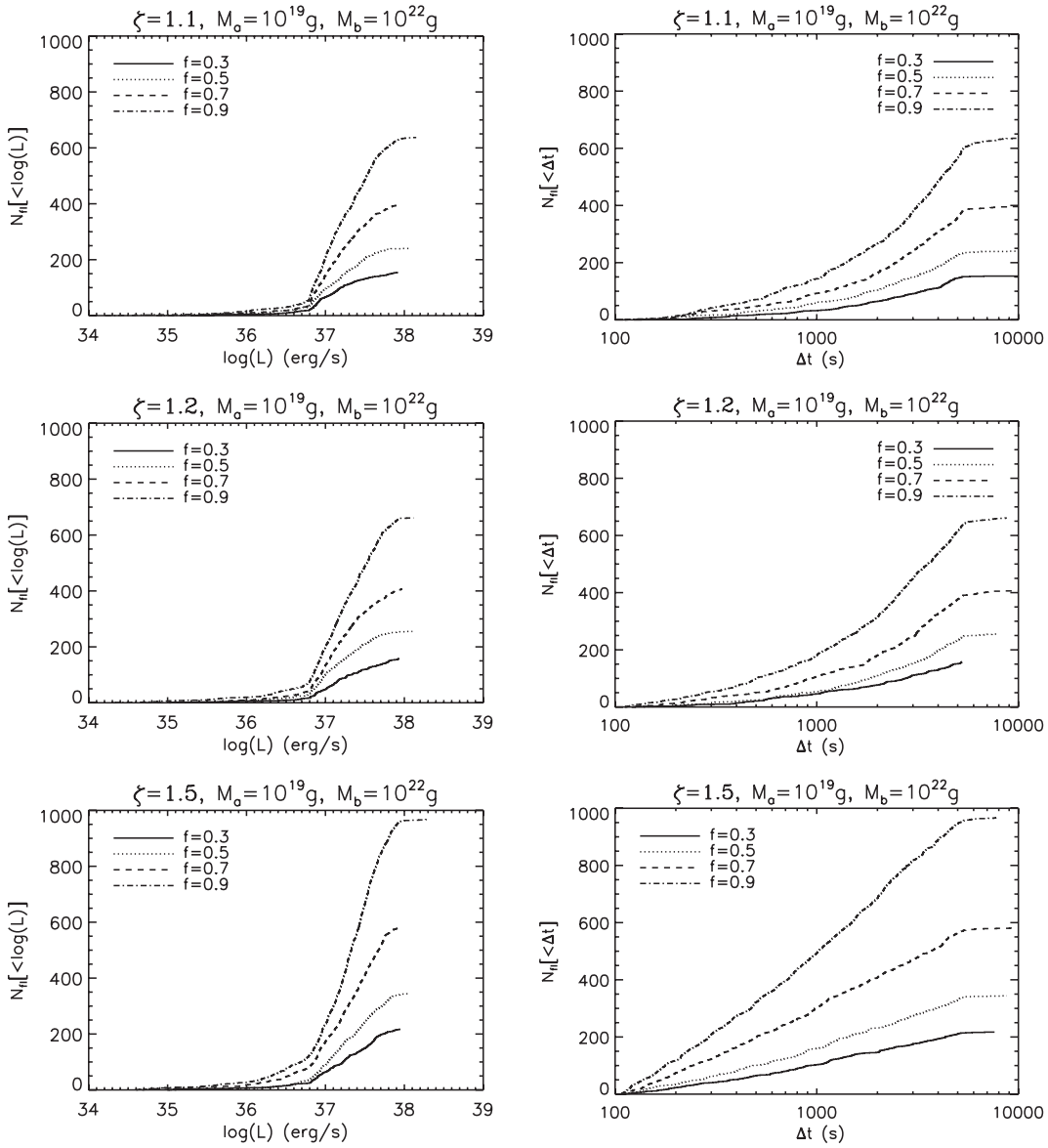

Figure 5. Expected integral distributions of the flare luminosities (left-hand panels) and durations (right-hand panels) for different values of $f = \dot{M}_{\rm cl}/\dot{M}_{\rm wind}$ and ζ. The binary system parameters are in the caption of Fig. 4. The time interval corresponds to 100 days.

were also obtained with $\gamma = 1$ and $\dot{M}_{\rm tot} = 4 \times 10^{-7}\,{\rm M}_{\odot}\,{\rm yr}^{-1}$, and with a normal distribution law for the clump radii, with $N_{\sigma} = 5$. We point out that the average luminosity observed by ASM/*RXTE* out of the flares is $\approx$3–4 $\times\ 10^{36}$ erg s^{-1}. This luminosity is obtained in our model with the accretion of numerous clumps with low density.

6 COMPARISON WITH THE HMXB 4U 1700−377

4U 1700−377 (Jones et al. 1973) is a 3.412-day eclipsing HMXB composed of a compact object (a neutron star or a black hole) and the O6.5 Iaf^{+} star HD 153919, located at a distance of 1.9 kpc (Ankay et al. 2001). Despite extensive searches, no X-ray pulsations have been found in this system. Therefore, the X-ray mass function cannot be determined and the system parameters ($M_{\rm OB}$, $R_{\rm OB}$, M_X) cannot be derived directly. They have been estimated from the radial velocity curve of the supergiant and from the duration of the X-ray eclipse, by making assumptions about possible values of the radius of the O star and the orbital inclination. Several studies indicate that the mass of the compact object is larger than 2 M$_{\odot}$ (Rubin et al. 1996; Clark et al. 2002). The similarity of the X-ray spectrum to other pulsars suggests that the compact object of 4U 1700−377 is a neutron star (White et al. 1983), but the presence of a low-mass black hole cannot be excluded (Brown, Weingartner & Wijers 1996). Reynolds et al. (1999) reported the presence of a possible cyclotron feature at ∼37 keV observed with *BeppoSAX*. If confirmed, this would demonstrate that 4U 1700−377 hosts a neutron star with a magnetic field of about 2.3 $\times\ 10^{12}$ G.

The X-ray light curve of 4U 1700−377 is characterized by a strong flaring activity with variations as large as a factor of 10–100 on time-scales from minutes to hours (White, Kallman & Swank 1983; Haberl, White & Kallman 1989; Rubin et al. 1996). We assumed the most recent set of system parameters of 4U 1700−377, obtained by means of a detailed non-local thermal equilibrium line-driven wind model analysis of HD 153919 and a Monte Carlo

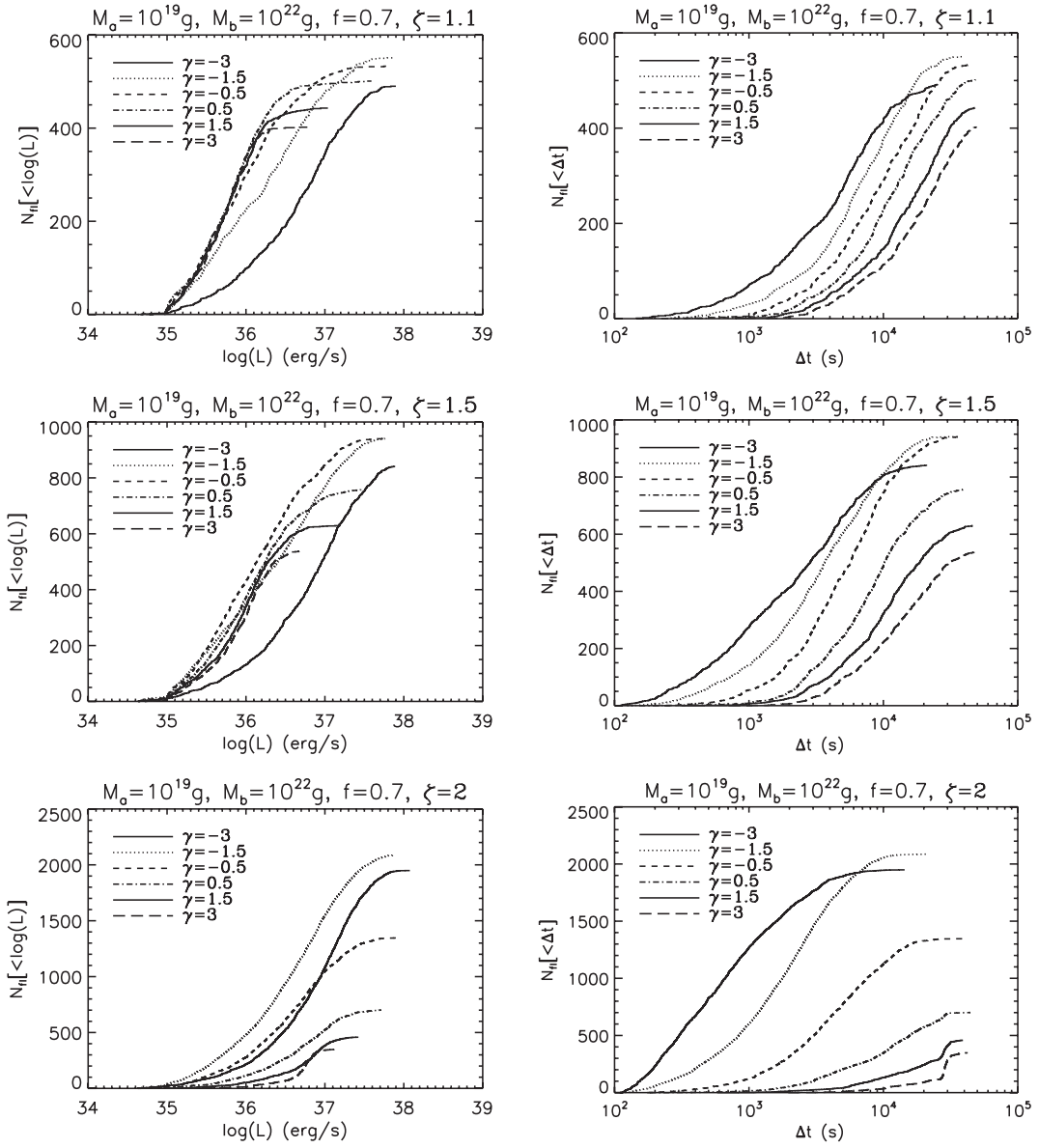

Figure 6. Expected integral distributions of the flare luminosities (left-hand panels) and durations (right-hand panels) for different values of γ and ζ of equations (10) and (1). The binary system parameters are in the caption of Fig. 4. The time interval for each histogram corresponds to 100 days.

simulation for the determination of the masses of both components (Clark et al. 2002). These authors found that the supergiant has a luminosity $\log(L/\mathrm{L}_\odot) = 5.82 \pm 0.07$, an effective temperature $T_{\rm eff} \approx$ 35 000 K, radius $R_{\rm OB} \approx 21.9\,\mathrm{R}_\odot$, mass $M_{\rm OB} \approx 58\,\mathrm{M}_\odot$, mass-loss rate $\dot{M} = 9.5 \times 10^{-6}\,\mathrm{M}_\odot\,\mathrm{yr}^{-1}$ and a mass for the compact object $M_{\rm X} = 2.44\,\mathrm{M}_\odot$ (Table 1).

The X-ray spectrum of 4U 1700−377 is well described by an absorbed power law with high-energy cut-off (van der Meer et al. 2005). The spectrum above 20 keV was studied using different satellites (e.g. BATSE detector on board the *Compton Gamma-ray Observatory*, *INTEGRAL*) and can be modelled using a thermal bremsstrahlung model with $kT \sim 25$ keV (Rubin et al. 1996) or with a thermal Comptonization model (Orr, Torrejón & Parmar 2004).

The analysis of the 0.5–12 keV spectrum with XMM-*Newton* during the eclipse, the egress and a low-flux interval led van der Meer et al. (2005) to suggest that the low-flux interval is probably due to a lack of accretion such as expected in a structured and inhomogeneous wind. Moreover, van der Meer et al. (2005) proposed that the fluorescence line from near-neutral iron detected in all spectra is produced by dense clumps. They also observed recombination lines during the eclipse which indicate the presence of ionized zone around the compact object.

We analysed the public archival *INTEGRAL* data of 4U 1700−377, using all the Imager on Board *INTEGRAL* Satellite/*INTEGRAL* Soft Gamma Ray Instrument observations obtained from 2003 March 12 to 2003 April 22, and from 2004 February 2 to 2004 March 1. These data correspond to a net exposure time of ∼5.2 days (excluding the eclipse phase). We reduced the data using OSA 7.0, and extracted the light curve in the energy range 15–60 keV, finding a total of 123 flares. For each flare, we extracted the spectrum in the range 22–100 keV. All the spectra could be well fit by a thermal Comptonization model (COMPTT in XSPEC). Based on the spectral results, we computed the 1–200 keV luminosity

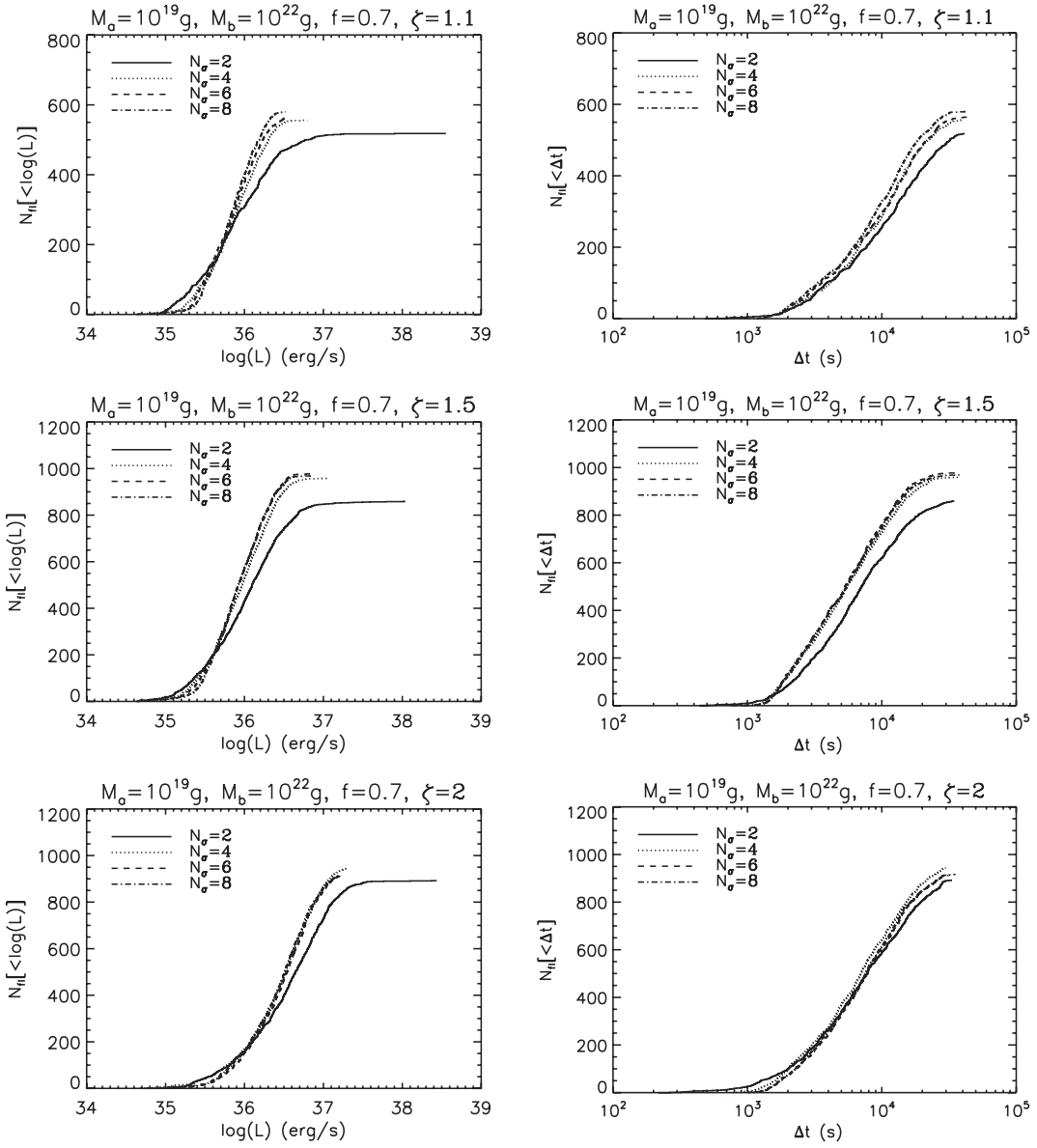

Figure 7. Expected integral distributions of the flare luminosities (left-hand panels) and durations (right-hand panels) for different values of N_σ and ζ of equations (11) and (1). The binary system parameters are in the caption of Fig. 4. The time interval for each histogram corresponds to 100 days.

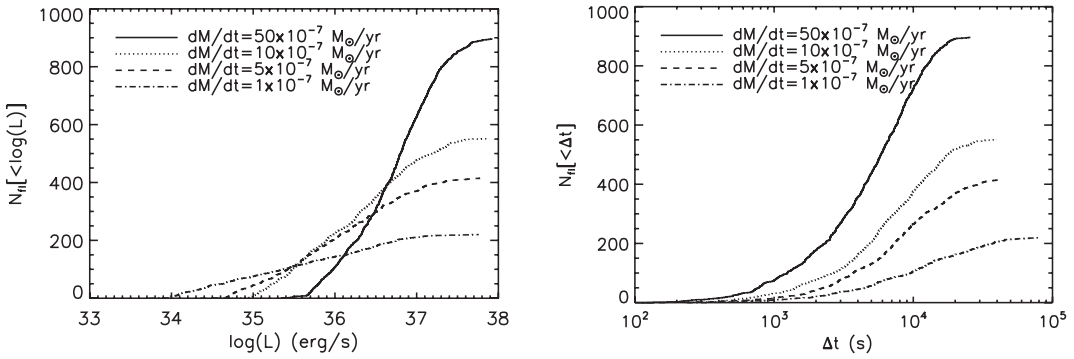

Figure 8. Expected integral distributions of the flare luminosities and durations for different values of the mass-loss rate and for an assumed orbital period of 10 days and a circular orbit. $\zeta = 1.1$, $\gamma = -1.5$, $f = 0.7$. The other binary system parameters are in the caption of Fig. 4. The time interval corresponds to 100 days.

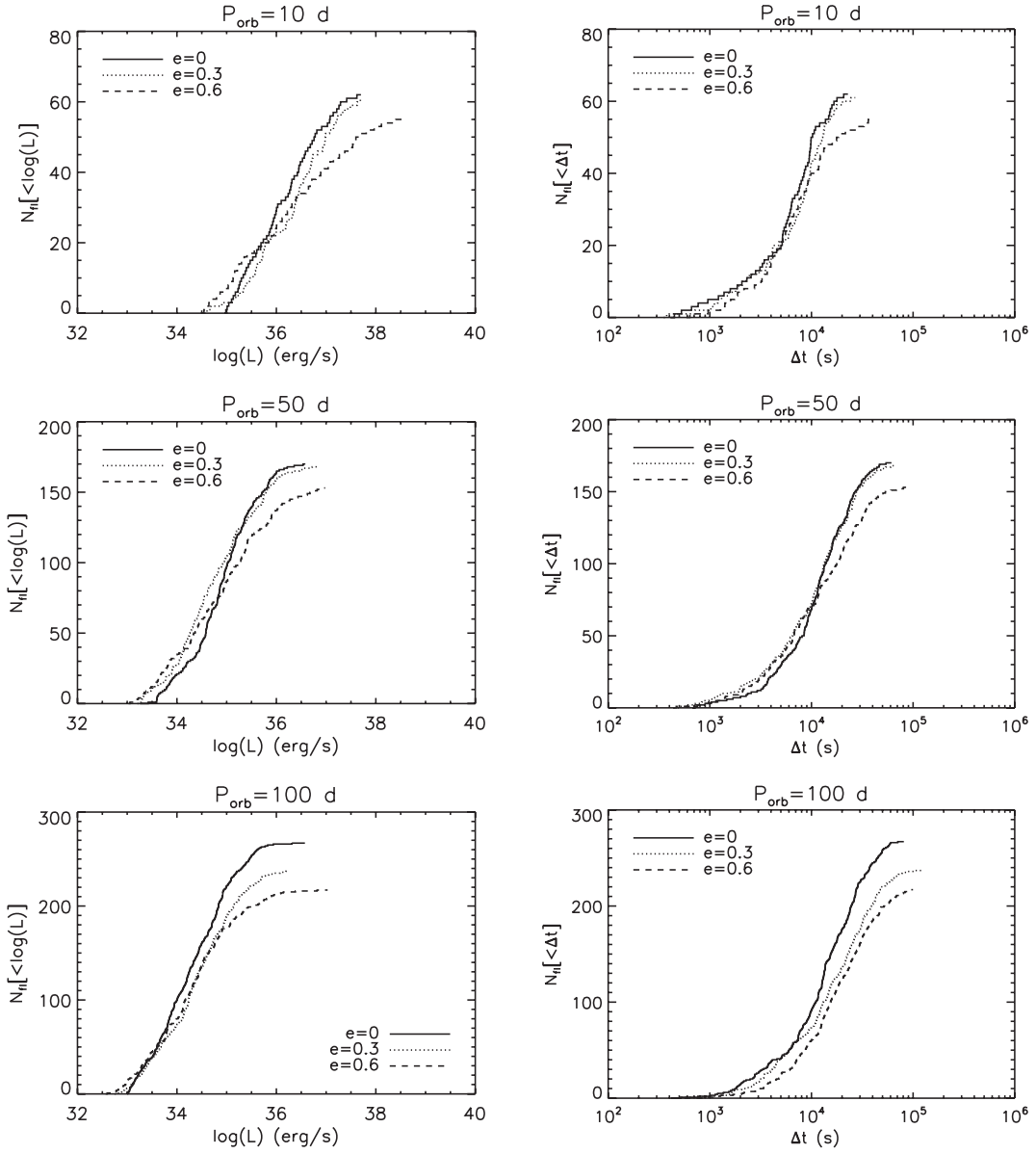

Figure 9. Expected integral distributions of the flare luminosities for different orbital periods and eccentricities of the binary system. $\zeta = 1.1$, $\gamma = -1.5$ and $f = 0.7$. The other binary system parameters are in the caption of Fig. 4. The time interval for each histogram corresponds to the orbital period.

of each flare. All of them have a luminosity greater than 5.8×10^{36} erg s^{-1} (for lower luminosities, it is difficult to evaluate the flare duration and then to distinguish the flares from the average level of the X-ray emission). For each flare, we have measured two parameters: the peak luminosity and the flare duration. We then applied our clumpy wind model to the *INTEGRAL* observations of 4U 1700−377. We first compared the observed distributions of the flare luminosities and durations with those computed adopting the system parameters reported in Table 1. We assumed for the computed distribution a time interval equal to the exposure time of the 4U 1700−377 observations considered here. As shown in Fig. 11, the flare properties are well reproduced with our clumpy wind model for $\dot{M}_{\rm tot} = 1.3 \times 10^{-6}\,{\rm M}_{\odot}\,{\rm yr}^{-1}$, $M_{\rm a} = 5 \times 10^{16}$ g and $M_{\rm b} = 2 \times 10^{19}$ g, $\zeta = 1.2$, $\gamma = -6.5$ and $f = 0.75$. We found that the numbers of observed (123) and calculated flares (116) are in good agreement. The light curve of 4U 1700−377 calculated with our clumpy wind model is shown in Fig. 12.

7 COMPARISON WITH THE SFXT IGR J11215−5952

The SFXT IGR J11215−5952 was discovered in 2005 April with *INTEGRAL* (Lubinski et al. 2005). It is associated with HD 306414, a B0.7 Ia star located at an estimated distance of ∼8 kpc (Negueruela et al. 2007). *RXTE* observations showed a pulse period $P_{\rm spin} = 186.78 \pm 0.3$ s (Smith, Bezayiff & Negueruela 2006; Swank, Smith & Markwardt 2007). This is the first SFXT for which a periodicity in the outbursts recurrence time was discovered (Sidoli, Paizis & Mereghetti 2006). Subsequent observations (Romano et al. 2009) showed that the true periodicity is about 164.5 days, i.e. half of the originally proposed value. This periodicity is very likely due to the orbital period of the system.

For a distance of 8 kpc, the peak fluxes of the outbursts correspond to a luminosity of $\sim 5 \times 10^{36}\,{\rm erg\,s^{-1}}$ (5–100 keV; Romano et al. 2007). *Swift* monitoring of this source revealed

Table 1. Parameters of the HMXBs studied in this paper.

	Vela X−1	4U 1700−377	IGR J11215−5952
Type	SGXB	SGXB	SFXT
Spectral type	B0.5 Ib	O6.5 Iaf$^+$	B0.7 Ia
$M_{\rm OB}$	23 $M_\odot$	58 $M_\odot$	23 $M_\odot$(*)
$R_{\rm OB}$	30 $R_\odot$	21.9 $R_\odot$	35.1 $R_\odot$(*)
$T_{\rm eff}$	2.5×10^4 K (*)	3.5×10^4 K	2.36×10^4 K (*)
$\log(L/L_\odot)$	5.58 (*)	5.82	5.5 (*)
$\dot{M}_{\rm tot}$	0.7–1.2 $\times 10^{-6}$ $M_\odot$ yr^{-1} (*)	9.5×10^{-6} $M_\odot$ yr^{-1}	1–2.5 $\times 10^{-6}$ $M_\odot$ yr^{-1}
v_∞	$\sim$ 1520–1600 km s^{-1} (*)	1700 km s^{-1}	$\sim$ 1000–1400 km s^{-1} (*) (†)
β	$\sim$ 1–1.5 (*)	1.3	$\sim$ 1–1.5
$M_{\rm NS}$	1.9 $M_\odot$	2.44 $M_\odot$	1.4 $M_\odot$
$P_{\rm orb}$	8.964 d	3.412 d	164.5 d
e	$e \sim 0.09$	0	–
$P_{\rm spin}$	$\sim$283 s	–	186.78 $\pm$ 0.3 s
Distance	$\sim$ 2.0 kpc	1.9 kpc	8 kpc

Note. Values labelled with (*) are taken from Searle et al. (2008) and values labelled with (†) are taken from Lefever et al. (2007).

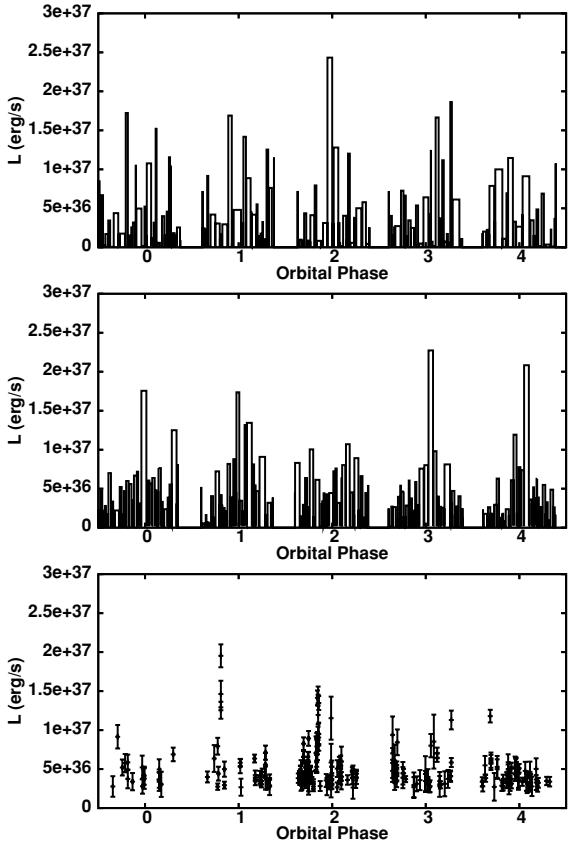

Figure 10. Comparison of the Vela X−1 light curve, as observed with ASM/*RXTE* (lower panel), with that calculated with our clumpy wind model for the parameters reported in Table 1, and $\dot{M}_{\rm tot} = 2.1 \times 10^{-7}$ $M_\odot$ yr^{-1}, $\beta = 1$, $v_\infty = 1600$ km s^{-1}, $f = \dot{M}_{\rm cl}/\dot{M}_{\rm wind} = 0.75$, $M_{\rm a} = 5 \times 10^{18}$ g, $M_{\rm b} = 5 \times 10^{21}$ g, $\zeta = 1.1$, $N_\sigma = 5$ (middle panel), and $\gamma = -1$ (upper panel), $k = 0.375$, $\alpha = 0.522$, $\delta = 0.099$. Orbital phase $\phi = 0$ corresponds to 53750 MJD. Note that Vela X−1 is not continuously observed with ASM/*RXTE*. Therefore, it is possible that some flares have been missed.

that the outburst (lasting a few days) is composed by many flares (lasting from minutes to a few hours), and before and after the whole outburst the source is fainter than 10^{33} erg s^{-1} (Sidoli et al. 2007).

Sidoli et al. (2007) showed that accretion from a spherically symmetric homogeneous wind could not reproduce the observed light curve, and therefore proposed a model based on an anisotropic wind characterized by a denser and slower equatorial component, periodically crossed by the neutron star along its orbit. However, this result was based on the old determination of the orbital period (329 days). Therefore, before applying our clumpy wind model, we checked the spherically symmetric homogeneous wind with $P_{\rm orb} = 164.5$ d, different eccentricity values, and the set of stellar parameters derived by Searle et al. (2008) and Lefever, Puls & Aerts (2007) and reported in Table 1. We assumed a terminal velocity v_∞ ranging from 1000 to 1400 km s^{-1}, and $\dot{M}$ ranging from 1×10^{-6} to 2.5×10^{-6} $M_\odot$ yr^{-1}. In all cases, we found that the duration of the X-ray outburst observed with *Swift* is shorter than that of the calculated light curves.

A better agreement with the observations could be obtained with our clumpy wind model, especially for what concerns the flaring variability during the outburst phase. However, also in this case the calculated light curve always produces an outburst longer than the observed one. This is shown in Fig. 13, where the green symbols correspond to the accretion of a dense clump (producing a flare), while the blue symbols indicate the lower luminosity level produced by the accretion of the interclump matter. We found that the probability to observe a flare, rather than the interclump luminosity level, is 90 per cent.

In order to improve the agreement between the observed and the calculated light curve, we introduced an anisotropic outflow similar to that proposed by Sidoli et al. (2007). In this modified model, we introduce a denser clumpy wind component in the equatorial plane, with a thickness $2h$, a terminal velocity $v_{\rm ed}$ and a mass-loss rate $\dot{M}_{\rm ed}$, together with a spherically symmetric clumpy wind component (polar wind) with terminal velocity $v_{\rm pw}$ and a mass-loss rate $\dot{M}_{\rm pw}$. We linked the mass-loss rate from the equatorial outflow with the mass-loss rate from the polar wind, by means of the factor of $f_{\rm ed}$:

$$\dot{M}_{\rm ed} = f_{\rm ed} \dot{M}_{\rm pw}. \quad (35)$$

Both wind components are clumpy and obey laws described in Section 2. We assume that the second wind component has a Gaussian density profile perpendicular to the equatorial plane of the supergiant. In this framework, we have considered an orbital period $P_{\rm orb} = 164.5$ d and a high eccentricity in order to produce only one

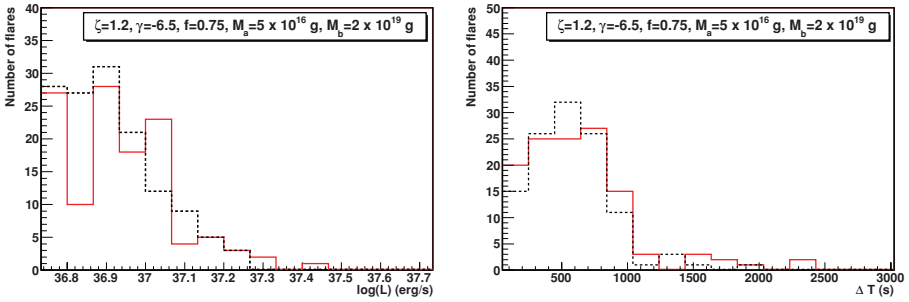

Figure 11. Comparison between observed (solid line) and calculated (dashed line) distributions of the flare luminosities and durations for 4U 1700−377. The binary system parameters are as follows: $M_{\rm OB} = 58\,{\rm M}_\odot$, $R_{\rm OB} = 21.9\,{\rm R}_\odot$, $M_{\rm NS} = 2.44\,{\rm M}_\odot$, $R_{\rm NS} = 10$ km. The parameters for the supergiant wind are as follows: $\dot{M}_{\rm tot} = 1.3 \times 10^{-6}\,{\rm M}_\odot\,{\rm yr}^{-1}$, $v_\infty = 1700\,{\rm km\,s}^{-1}$, $\beta = 1.3$, $v_0 = 10\,{\rm km\,s}^{-1}$, $M_{\rm a} = 5 \times 10^{16}$ g and $M_{\rm b} = 2 \times 10^{19}$ g, $\zeta = 1.2$, $\gamma = -6.5$ and $f = 0.75$.

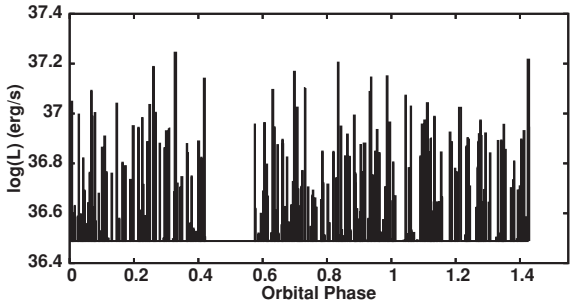

Figure 12. Computed light curve of 4U 1700−377. The off-state at orbital phase $0.42 \lesssim \phi \lesssim 0.58$ is due to the eclipse. The stellar parameters are reported in the caption of Fig. 11.

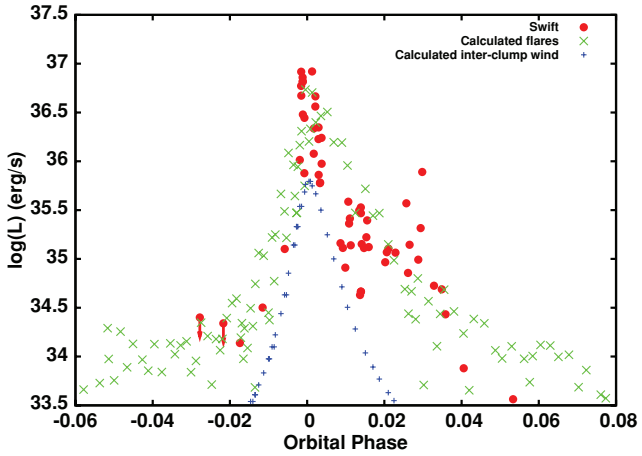

Figure 13. Comparison of the IGR J11215−5952 light curve of the 2007 February outburst observed with *Swift*/XRT with the calculated X-ray light curve of our clumpy wind model (presented in Section 2) with the stellar parameters reported in Table 1, and $P_{\rm orb} = 164.5$ d, $e = 0.89$, $\dot{M}_{\rm tot} = 2 \times 10^{-7}\,{\rm M}_\odot\,{\rm yr}^{-1}$, $\beta = 1$, $v_\infty = 1400\,{\rm km\,s}^{-1}$, $f = \dot{M}_{\rm cl}/\dot{M}_{\rm wind} = 0.75$, $M_{\rm a} = 10^{17}$ g, $M_{\rm b} = 10^{20}$ g, $\zeta = 1.1$, $\gamma = 6$, $k = 0.709$, $\alpha = 0.470$, $\delta = 0.089$.

outburst per orbit. The comparison between the *Swift* light curve and that predicted with this model is shown in Fig. 14. A good agreement with the data is obtained with the parameters reported in Table 2.

8 DISCUSSION AND CONCLUSIONS

We have developed a clumpy wind model (where the dynamical problem is not treated) and explored the resulting effects on an accreting compact object in order to explain the observed behaviour of the SFXTs and the supergiant X-ray binaries (SGXBs). Compared to the previous attempts to explain the SFXT outbursts in the context of clumpy winds (Walter & Zurita Heras 2007; Negueruela et al. 2008), we introduced a distribution for the masses and initial dimensions of the clumps. We described the subsequent expansion of the clumps (equation 9) taking into account realistic upper and lower limits for their radius (equations 20 and 25).

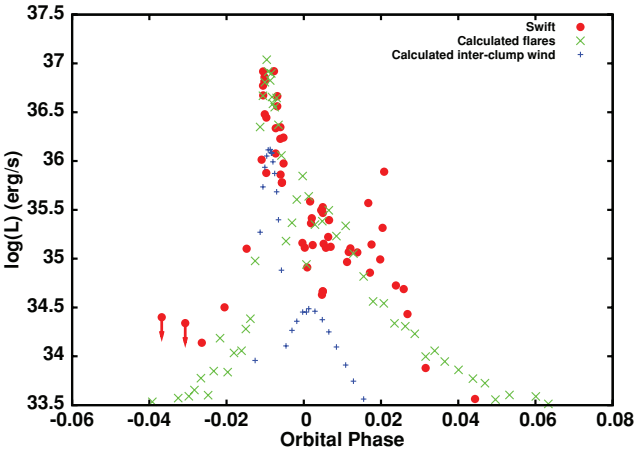

Figure 14. Comparison of the IGR J11215−5952 light curve of the 2007 February outburst observed with *Swift*/XRT with the calculated X-ray light curve of our clumpy wind model with equatorially enhanced wind component (presented in Section 2). We used the stellar parameters reported in Table 2.

This model, together with the theory of wind accretion modified because of the presence of clumps, allows a comparison with the observed properties of both the light curves and luminosity distributions of the flares in SGXBs and SFXTs.

From the calculated integral distributions (Section 4), we found that the observable characteristics of the flares, such as luminosity, duration, number of flares produced, depend mainly on the orbital period (Fig. 9), the scaling parameter ζ of the power-law distribution for the clump formation rate (equation 1) and the fraction of wind mass in the form of clumps ($f = \dot{M}_{\rm cl}/\dot{M}_{\rm tot}$), as shown in Figs 4 and 5. Thus, the variability properties of the different systems do not depend only on the orbital parameters but are also significantly affected by the properties of the clumps (in particular by the parameters ζ, γ, f, $M_{\rm a}$, $M_{\rm b}$).

We successfully applied our clumpy wind model to three different HMXBs: Vela X−1, 4U 1700−377 and IGR J11215−5952. For the latter source, however, we had to introduce a denser equatorial

Table 2. Parameters for the calculated X-ray light curves of IGR J11215−5952 of our clumpy wind model with equatorially enhanced wind component (see Fig. 14).

Parameter	Value
β	1
$\dot{M}_{\rm pw}$	$1 \times 10^{-7}\,{\rm M}_\odot\ {\rm yr}^{-1}$
$v_{\infty,{\rm pw}}$	$1500\ {\rm km\,s}^{-1}$
i_0	20°
$i_{\rm p}$	70°
$h_{\rm ed}$	2.0×10^{11} cm
$f = \dot{M}_{\rm cl}/\dot{M}_{\rm wind}$	0.75
$M_{\rm a}$	5×10^{18} g
$M_{\rm b}$	10^{20} g
ζ	1.1
γ	6
$f_{\rm ed}$	100
$v_{\infty,{\rm ed}}$	$1000\ {\rm km\,s}^{-1}$

Note. i_0 is the angle of inclination of the orbital plane with respect the equatorial wind component; $i_{\rm p}$ is the angle between the orbital plane intersection with the equatorial wind component and the direction of the periastron.

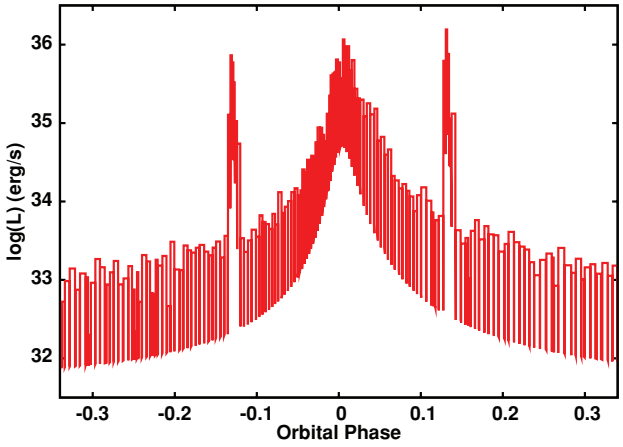

Figure 15. Calculated light curve of an SFXT with a neutron star accreting an anisotropic clumpy wind. The parameters of the system are as follows: $M_{\rm NS} = 1.4\,{\rm M}_\odot$, $M_{\rm OB} = 23\,{\rm M}_\odot$, $R_{\rm OB} = 35.1\,{\rm R}_\odot$, $L_{\rm OB} = 3.16 \times 10^5\,{\rm L}_\odot$, $P_{\rm orb} = 80$ d, $e = 0.75$, $\dot{M}_{\rm tot} = 2 \times 10^{-7}\,{\rm M}_\odot\ {\rm yr}^{-1}$, $v_{\infty,{\rm pw}} = 1500\ {\rm km\,s}^{-1}$, $\beta = 1$, $i_0 = 15^\circ$, $i_{\rm p} = 0^\circ$, $h = 2.0 \times 10^{11}$ cm, $v_{\infty,{\rm ed}} = 1000\ {\rm km\,s}^{-1}$, $f_{\rm ed} = 50$, $T_{\rm eff} = 20000$ K, k = 0.709, $\alpha = 0.470$, $\delta = 0.089$, $\zeta = 1.1$, $\gamma = 6$, $M_{\rm a} = 5 \times 10^{18}$ g, $M_{\rm b} = 10^{20}$ g.

component (still with a clumpy structure) in order to reproduce the flare duration.

In Fig. 15, we show an example of a light curve of a generic SFXT calculated in the case of anisotropic clumpy wind. We assume for the generic SFXT properties similar to IGR J11215−5952, with an orbital period of 80 days and an eccentricity $e = 0.75$. The orbital plane intersects the equatorial wind component at two phases ($\phi_1 \approx -0.12$, $\phi_2 \approx 0.12$) producing two outbursts. The third outburst is produced at the periastron passage ($\phi_3 \approx 0$). This implies that, if this explanation is correct, up to three outbursts per orbit are possible.

In Table 3, we have summarized the wind parameters obtained for the three sources. This table shows the typical differences in the mass-loss rate and terminal velocity expected from the CAK theory, similar values for ζ and f, and different values for γ, $M_{\rm a}$, $M_{\rm b}$, which seem to be proportional to the inverse of the effective temperature of the supergiant. Moreover, we found that the values of $\dot{M}_{\rm tot}$ that best reproduce the observed light curves of the three HMXBs studied are in agreement with the hypothesis that the mass-loss rate derived by the Hα emission is overestimated by a factor of 2–10, in agreement with the recent studies (see Section 4.3). We can exclude that the observed light curves of the three HMXBs studied can be reproduced with the same set of wind parameters.

In conclusion, the different values of γ, $M_{\rm a}$, $M_{\rm b}$ obtained for the three HMXBs studied in this paper reveal that, in the framework of our clumpy wind model, the properties of the clumps of these three X-ray binary systems are slightly different, independently of the orbital period. This discrepancy could be due to the different spectral types of the three supergiants, which could eject structurally inhomogeneous winds with slightly different properties. We suggest as a possible cause of this behaviour that the values of γ, $M_{\rm a}$, $M_{\rm b}$ could be related to the sonic radius where the clumps start (Bouret et al. 2005), which depends on the supergiant properties (equation 8).

ACKNOWLEDGMENTS

LD thanks Professor A. Treves for very helpful discussions. We thank the referee (L. B. Lucy) for useful comments which helped in significantly improving our paper. This work was supported in Italy by ASI contracts I/023/05/0, I/088/06/0 and I/008/07/0.

REFERENCES

Abbott D. C., 1982, ApJ, 259, 282
Ankay A., Kaper L., de Bruijne J. H. J., Dewi J., Hoogerwerf R., Savonije G. J., 2001, A&A, 370, 170
Bondi H., Hoyle F., 1944, MNRAS, 104, 273
Bouret J.-C., Lanz T., Hillier D. J., 2005, A&A, 438, 301
Bozzo E., Falanga M., Stella L., 2008, ApJ, 683, 1031
Brown G. E., Weingartner J. C., Wijers R. A. M. J., 1996, ApJ, 463, 297
Brucato R. J., Kristian J., 1972, ApJ, 173, L105
Carlberg R. G., 1980, ApJ, 241, 1131
Castor J. I., Abbott D. C., Klein R. I., 1975, ApJ, 195, 157 (CAK)
Clark J. S., Goodwin S. P., Crowther P. A., Kaper L., Fairbairn M., Langer N., Brocksopp C., 2002, A&A, 392, 909
Davidson K., Ostriker J. P., 1973, ApJ, 179, 585
Grebenev S. A., Sunyaev R. A., 2007, Astron. Lett., 33, 149
Haberl F., 1994, A&A, 288, 791
Haberl F., White N. E., Kallman T. R., 1989, ApJ, 343, 409

Table 3. Summary of HMXBs studied in this paper. We give in the table their name, type (SGXB or SFXT), spectral type, the nature of the compact object and wind parameters that we have assumed. For IGR J11215−5952, the terminal velocity in the polar wind region is reported.

Source	Type	Supergiant	Compact object	$\dot{M}_{\rm tot}$ (${\rm M}_\odot\ {\rm yr}^{-1}$)	v_∞ (${\rm km\,s}^{-1}$)	ζ	γ	f	$M_{\rm a}$ (g)	$M_{\rm b}$ (g)
Vela X−1	SGXB	B0.5 Ib	NS	2.1×10^{-7}	1600	1.1	−1	0.75	5×10^{18}	5×10^{21}
4U 1700−377	SGXB	O6.5 Iaf$^+$	NS?	1.3×10^{-6}	1700	1.2	−6.5	0.75	5×10^{16}	2×10^{19}
IGR J11215−5952	SFXT	B0.7 Ia	NS	1×10^{-7}	1500	1.1	6	0.75	5×10^{18}	10^{20}

Hamann W.-R., Feldmeier A., Oskinova L. M., eds, 2008, Proc. Int. Workshop, Clumping in Hot-Star Winds. University of Potsdam, Potsdam, p. 11
Howk J. C., Cassinelli J. P., Bjorkman J. E., Lamers H. J. G. L. M., 2000, ApJ, 534, 348
Hoyle F., Lyttleton R. A., 1939, Proc. Cambridge Philosophical Soc., Vol. 34, The Effect of Interstellar Matter on Climatic Variation. Cambridge Philosophical Society, Cambridge, p. 405
in't Zand J. J. M., 2005, A&A, 441, L1
Jones C., Forman W., Tananbaum H., Schreier E., Gursky H., Kellogg E., Giacconi R., 1973, ApJ, 181, L43
Kreykenbohm I. et al., 2008, A&A, 492, 511
Kudritzki R.-P., Puls J., 2000, ARA&A, 38, 613
Kudritzki R. P., Pauldrach A., Puls J., Abbott D. C., 1989, A&A, 219, 205
Lamers H. J. G. L. M., Cassinelli J. P., 1999, in Henny J. G. L. M. Lamers and Joseph P. Cassinelli, eds, Introduction to Stellar Winds. Cambridge Univ. Press, Cambridge, p. 452 (ISBN 0521593980)
Lefever K., Puls J., Aerts C., 2007, A&A, 463, 1093
Lépine S., Moffat A. F. J., 2008, AJ, 136, 548
Lubinski P., Bel M. G., von Kienlin A., Budtz-Jorgensen C., McBreen B., Kretschmar P., Hermsen W., Shtykovsky P., 2005, ATel, 469, 1
Lucy L. B., Solomon P. M., 1970, ApJ, 159, 879
Lucy L. B., White R. L., 1980, ApJ, 241, 300
Negueruela I., Smith D. M., Reig P., Chaty S., Torrejón J. M., 2006, in Wilson A., ed., Proc. of 'The X-ray Universe 2005', ESA SP-604. ESA, Noordwijk, p. 165
Negueruela I., Smith D. M., Torrejon J. M., Reig P., 2007, in Grebenev S., Sunyaev R., Winkler C., eds, Proc. 6th Integral Workshop-The Obscure, ESA SP-622. ESA, Noordwijk, p. 255
Negueruela I., Torrejón J. M., Reig P., Ribó M., Smith D. M., 2008, in Bandyopadhyay R. M., Wachter S., Gelino D., Gelino C. R., eds, AIP Conf. Ser., Vol. 1010, A Population Explosion: The Nature & Evolution of X-ray Binaries in Diverse Environments. Am. Inst. Phys., New York, p. 252
Orlandini M. et al., 1998, A&A, 332, 121
Orr A., Torrejón J. M., Parmar A. N., 2004, in Schoenfelder V., Lichti G., Winkler C., eds, 5th Integral Workshop on the Integral Universe, ESA SP-552. ESA, Noordwijk, p. 361
Oskinova L. M., Hamann W.-R., Feldmeier A., 2007, A&A, 476, 1331
Owocki S. P., Castor J. I., Rybicki G. B., 1988, ApJ, 335, 914
Puls J. et al., 1996, A&A, 305, 171
Reynolds A. P., Owens A., Kaper L., Parmar A. N., Segreto A., 1999, A&A, 349, 873
Romano P., Sidoli L., Mangano V., Mereghetti S., Cusumano G., 2007, A&A, 469, L5
Romano P., Sidoli L., Cusumano G., Vercellone S., Mangano V., Krimm H. A., 2009, ApJ, 696, 2068
Rubin B. C. et al., 1996, ApJ, 459, 259
Runacres M. C., Owocki S. P., 2002, A&A, 381, 1015
Runacres M. C., Owocki S. P., 2005, A&A, 429, 323
Sadakane K., Hirata R., Jugaku J., Kondo Y., Matsuoka M., Tanaka Y., Hammerschlag-Hensberge G., 1985, ApJ, 288, 284
Sako M., Liedahl D. A., Kahn S. M., Paerels F., 1999, ApJ, 525, 921
Searle S. C., Prinja R. K., Massa D., Ryans R., 2008, A&A, 481, 777
Sguera V. et al., 2005, A&A, 444, 221
Shimada M. R., Ito M., Hirata B., Horaguchi T., 1994, in Balona L. A., Henrichs H. F., Le Contel J. M., eds, Proc. IAU Symp. 162, Pulsation; Rotation; and Mass Loss in Early-Type Stars. Kluwer, Dordrecht, p. 487
Sidoli L., 2009, Adv. Space Res., 43, 1464
Sidoli L., Paizis A., Mereghetti S., 2006, A&A, 450, L9
Sidoli L., Romano P., Mereghetti S., Paizis A., Vercellone S., Mangano V., Götz D., 2007, A&A, 476, 1307
Sidoli L. et al., 2008, ApJ, 687, 1230
Smith D. M., Bezayiff N., Negueruela I., 2006, ATel, 773, 1
Swank J. H., Smith D. M., Markwardt C. B., 2007, ATel, 999, 1
Vacca W. D., Garmany C. D., Shull J. M., 1996, ApJ, 460, 914
van der Meer A., Kaper L., di Salvo T., Méndez M., van der Klis M., Barr P., Trams N. R., 2005, A&A, 432, 999
van Kerkwijk M. H., van Paradijs J., Zuiderwijk E. J., Hammerschlag-Hensberge G., Kaper L., Sterken C., 1995, A&A, 303, 483
Walter R., Zurita Heras J., 2007, A&A, 476, 335
White N. E., Kallman T. R., Swank J. H., 1983, ApJ, 269, 264

This paper has been typeset from a TEX/LATEX file prepared by the author.